AIAA JOURNAL
Vol. 30, No. 12, December 1992

Postbuckling Response of Stiffened Composite Cylindrical Shells

Srinivasan Sridharan* and Madjid Zeggane†
Washington University, St. Louis, Missouri 63130
and
James H. Starnes Jr.‡
NASA Langley Research Center, Hampton, Virginia 23665

The local buckling and the associated postbuckling response of stiffened composite shells are studied using an asymptotic approach. Both the classical (Kirchhoff) theory (CPT) and a first-order shear deformation theory (SDT) are employed in the study. SDT analysis was carried out using p-version type finite strips, whereas CPT analysis employed h-version based strips. Convergence studies confirm the superiority of the p-version approach. A panel width-to-thickness ratio of 50 was chosen to investigate the influence of shear deformation for stiffened and isolated panels fabricated out of isotropic and composite layered materials. The shear deformation effects were significant for composite stiffened shell panels with CPT giving a noticeably stiffer response. In comparison with isotropic shell panels, orthotropic layered panels buckle at lower nondimensional buckling loads but are appreciably less sensitive to imperfection.

Nomenclature

A_{ij}, B_{ij}, D_{ij} = constitutive relationship matrices for a composite laminate
b = width of the panel (stiffener spacing)
b^* = imperfection-sensitivity parameter
d_s = depth of the stiffener
E_1, E_2 = elastic moduli of a lamina in the fiber and transverse directions, respectively
E_x = effective modulus of the whole structure
$\bar{E}_x$ = effective modulus of the x direction at any location
G_{12} = inplane shear modulus of a lamina
$\bar{G}$ = averaged out-of-plane shear modulus of laminate
h = thickness of laminate
L = length of the structure
ℓ = half-wave length of buckling
m = number of half-waves of buckling
n = number of elements
p = degree of the polynomial displacement functions
R = radius of the shell
t = thickness of the shell
t_s = thickness of the stiffener
u, v, w = displacement components in the longitudinal, transverse, and out-of-plane directions, respectively
α, β = rotations of the normal in the xz and yz planes, respectively
λ = total end-shortening divided by L
λ_{cr} = critical value of λ
λ_2 = second-order component of λ
ξ = scaling parameter for the buckling mode
σ_{cr} = critical stress (averaged)
σ_{av} = averaged axial stress
$\bar{\sigma}$ = σ_{av}/E_x
σ_2^{ef} = second-order component of σ_{av} [see Eq. (24)]
$\bar{\sigma}_2$ = σ_2^{ef}/E_x

Received Jan. 21, 1992; revision received April 20, 1992; accepted for publication May 13, 1992.
*Professor, Department of Civil Engineering. Member AIAA.
†Graduate Student, Department of Civil Engineering.
‡Head, Aircraft Structures Branch. Associate Fellow AIAA.

Introduction

THE problems of local buckling and imperfection sensitivity of compressed stiffened panels fabricated out of isotropic materials have been extensively studied in literature (see, for example, Refs. 1-6). The increasing use of laminated composites in the aerospace industry has given a fresh impetus and a new direction to the study of buckling and postbuckling responses of stiffened panels. A comprehensive review of the state of the art of laminated shell analysis is available in Ref. 7. The composite structures differ from the isotropic metallic structures by virtue of anisotropy and high shear deformability. The discrepancies in the buckling loads of moderately thick composite plates that arise due to the application of classical plate theory (CPT) have been highlighted by the authors in earlier papers.[8,9] The present paper treats not only buckling but also postbuckling responses of stiffened cylindrical shell panels undergoing local buckling. Though interesting in itself, the post-local-buckling behavior is of greater interest as a vital ingredient in the description of modal interaction, a subject of paramount importance in the optimal design of stiffened structures.

Both CPT and first-order shear deformation theory (SDT) are used in the analyses, so that the effect of shear deformation can be appreciated by comparison. The structure is considered to be sufficiently long in comparison with the wavelength of local buckles so that kinematic boundary conditions at the ends of the structure are of no consequence. Thus the variation of the displacement components in the longitudinal ($-x$) direction can be described in terms of "exact" trigonometric functions that satisfy the governing differential equations. Discretization is thus confined to the transverse direction, where appropriate polynomials are employed as displacement functions. For the postbuckling analysis, an asymptotic approach is used; this involves the computation of the second-order fields in terms of the buckling mode. (The asymptotic approach has been succinctly presented by Budiansky.[10] Several applications of the asymptotic theory to shell problems have been summarized by Bushnell in a relatively recent monograph.[11]) In all of the calculations based on SDT, a p-version approach (with a relatively small number of elements) is employed to eliminate the effect of shear locking, whereas the h-version approach is used for the CPT calculations.

For simplicity, attention is focused in this paper on problems of stiffened shells fabricated from specially orthotropic laminates and subject to prescribed uniform end-shortening. The study investigates the discrepancies between descriptions

of behavior as produced, respectively, by CPT and SDT and illustrates the divergences in behavior of stiffened panels fabricated from isotropic and orthotropic materials, respectively.

Theory

Problem Definition

The cross section of a typical stiffened shell panel is shown in Fig. 1. The actual shell structure is assumed to be composed of a sequence of many such panels placed side by side. The loading takes the form of prescribed uniform end-shortening, given by a single parameter, $\lambda(=\Delta/L)$, where Δ is the total end-shortening. We are interested in the critical value of $\lambda(\lambda_{cr})$ associated with local buckling and the postbuckling responses in the immediate vicinity of bifurcation, including the possible imperfection sensitivity of the panel.

Displacement, Strain, and Stress Vectors

The SDT formulation is based on the well-known Reissner-Mindlin theory. Thus we define the vectors of displacement, strain, and stress in the following manner:

$$\{u\}^T = \{u,\ v,\ w,\ \alpha,\ \beta\} \tag{1a}$$

$$\{\epsilon\}^T = \{\epsilon_x,\ \epsilon_y,\ \gamma_{xy},\ \chi_x,\ \chi_y,\ \chi_{xy},\ \gamma_{xy},\ \gamma_{yz}\} \tag{1b}$$

$$\{\sigma\}^T = \{N_x,\ N_y,\ N_{xy},\ M_x,\ M_y,\ M_{xy},\ Q_x,\ Q_y\} \tag{1c}$$

ϵ_x, ϵ_y, and γ_{xy} are the in-plane strain components and designated as ϵ_1, ϵ_2, and ϵ_6, respectively; χ_x, χ_y, and χ_{xy} are the out-of-plane curvature components and designated as χ_1, χ_2, and χ_6, respectively; and γ_{xz} and γ_{yz} are the transverse shearing strains and designated as γ_1, and γ_2, respectively. The σ consists of the corresponding stress resultants, viz., the in-plane forces N_1, N_2, and N_6, moments M_1, M_2, and M_6, and transverse shear forces Q_1 and Q_2 carried by the plate per unit length. The notation employed here is the same as in Ref. 12.

Stress-Strain Relationships

The relationship between σ and ϵ for the composite laminate can be expressed in the following form:

$$\begin{Bmatrix} N_i \\ M_i \end{Bmatrix} = \begin{bmatrix} A_{ij} & B_{ij} \\ B_{ij} & D_{ij} \end{bmatrix} \begin{Bmatrix} \epsilon_j \\ \chi_j \end{Bmatrix} \qquad (i, j = 1, 2, 6)$$

$$Q_l = k\bar{G}t\gamma_l \qquad (l = 1, 2) \tag{2a–c}$$

where k is the shear-correction factor (taken as 5/6). Equations (2a–2c) may be written in abbreviated form as $\sigma_i = H_{ij}\epsilon_j$.

Kinematics

Reissner-Mindlin Hypothesis

The in-plane displacement components u_z and v_z at any distance z from the middle surface are expressed in the form

$$u_z = u(x, y) + z\alpha(x, y) \tag{3a}$$

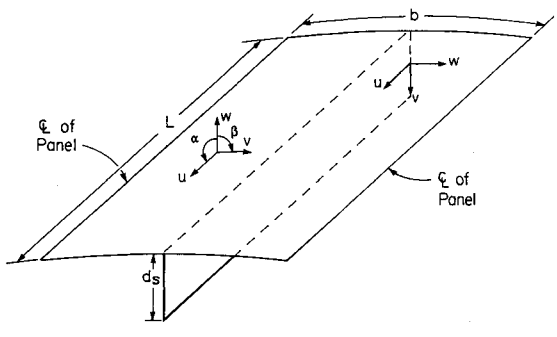

Fig. 1 Stiffened panel (from center to center of shell) with dimensions and axes of coordinates.

$$v_z = v(x, y) + z\beta(x, y) \tag{3b}$$

Strain-Displacement Relations

The following strain-displacement relations are used in the present treatment:

$$\epsilon_x = \frac{\partial u}{\partial x} + \frac{1}{2}\left(\frac{\partial w}{\partial x}\right)^2 \tag{4a}$$

$$\epsilon_y = \left(\frac{\partial v}{\partial y}\right) + \frac{w}{R} + \frac{1}{2}\left(\frac{\partial w}{\partial y}\right)^2 \tag{4b}$$

$$\gamma_{xy} = \left(\frac{\partial u}{\partial y}\right) + \left(\frac{\partial v}{\partial x}\right) + \frac{\partial w}{\partial x}\frac{\partial w}{\partial y} \tag{4c}$$

$$\chi_x = \frac{\partial \alpha}{\partial x} \tag{4d}$$

$$\chi_y = \frac{\partial \beta}{\partial y} \tag{4e}$$

$$\chi_{xy} = \frac{\partial \alpha}{\partial y} + \frac{\partial \beta}{\partial x} \tag{4f}$$

The transverse shear strains take the form

$$\gamma_{xz} = \alpha + \frac{\partial w}{\partial x} \tag{5a}$$

$$\gamma_{yz} = \beta + \frac{\partial w}{\partial y} \tag{5b}$$

Equations (3–5) may be viewed as Donnell's theory[13] for shallow cylindrical shells modified to account for shear deformation. The CPT formulation is obtained from these equations by simply setting $\alpha = -\partial w/\partial x$ and $\beta = -\partial w/\partial y$ and eliminating Q_x and Q_y from the stress vector σ.

Equations (4) and (5) may be written in the following form[10]:

$$\epsilon_i = L_{1_{ij}}(u_j) + \tfrac{1}{2}L_{2_{ij}}(u_j) \tag{6}$$

where L_1 and L_2 are, respectively, linear and quadratic operators. Further, a bilinear operator L_{11} is defined with respect to any two displacement vectors u_i and u_i' as in

$$L_{2_{ij}}(u_j + u_j') = L_{2_{ij}}(u_j) + 2L_{11_i}(u_j + u_j') + L_{2_{ij}}(u_j') \tag{7}$$

Potential Energy Function and Equations of Equilibrium

Each of u, ϵ, and σ are viewed as a sum of two contributions, one due to the prebuckling state and the other associated with the buckling process. Thus,

$$u = u^0 + u^* \tag{8a}$$

$$\epsilon = \epsilon^0 + \epsilon^* \tag{8b}$$

$$\sigma = \sigma^0 + \sigma^* \tag{8c}$$

where the superscripts 0 and * stand for the contributions of the unbuckled state and that of the buckling process, respectively. Note that, for our problem, $\sigma_1^0 = N_x^0 = -\lambda\bar{E}_x h$, where $\bar{E}_x$ and h are, respectively, the effective elastic modulus and thickness of the laminate in any location and $\sigma_i^0 = 0$, for $i \neq 1$. The prebuckling path is assumed to be linear, i.e., $\sigma_i^0 \cdot L_{11_i}(u_j^0 + u_j') = 0$ for all i and j and any u_j' where a dot operation indicates multiplication and integration over the entire surface of the structure.

With these definitions the total potential energy of the structure with a linear prebuckling path can be expressed in the following form:

$$\Pi = \tfrac{1}{2}\{H_{ij}[L_{1_{ik}}(u_k^*)\cdot L_{1_{jl}}(u_l^*) + L_{1_{ik}}(u_k^*)\cdot L_{2_{jl}}(u_l^*) + \tfrac{1}{4}L_{2_{ik}}(u_k^*)\cdot L_{2_{jl}}(u_l^*)] + \sigma_i^0\cdot L_{2_{ik}}(u_k^*)\} \quad (i, j = 1, \ldots, 8, \quad k, l = 1, \ldots, 5) \tag{9}$$

Equations of equilibrium are obtained by invoking the principle of stationary potential energy. Thus,

$$\delta\Pi = H_{ij}[L_{1_{ik}}(u_k^*) + \tfrac{1}{2}L_{2_{ik}}(u_k^*)]\cdot[L_{1_{jl}}(\delta u_l) + L_{11_j}(u_l^*, \delta u_l)] + \sigma_i^0\cdot L_{11_i}(u_k^*, \delta u_k) = 0 \quad (i, j = 1, \ldots, 8, \quad k, l = 1, \ldots, 5) \tag{10}$$

Asymptotic Approach

The generic displacement, stress, and strain associated with buckling are each taken in the following form:

$$u^* = u^{(1)}\xi + u^{(2)}\xi^2 + u^{(3)}\xi^3 + \cdots \tag{11a}$$

$$\epsilon^* = \epsilon^{(1)}\xi + \epsilon^{(2)}\xi^2 + \epsilon^{(3)}\xi^3 + \cdots \tag{11b}$$

$$\sigma^* = \sigma^{(1)}\xi + \sigma^{(2)}\xi^2 + \sigma^{(3)}\xi^3 + \cdots \tag{11c}$$

where ξ is a parameter that measures the growth of the buckling deformation. The vectors, $u^{(1)}$, $\epsilon^{(1)}$, and $\sigma^{(1)}$ (the first-order quantities) are given by the buckling mode while the terms $u^{(2)}$, $\epsilon^{(2)}$, and $\sigma^{(2)}$ give the respective second-order field. Once evaluated, these can be used to give the postbuckling stiffness in the vicinity of bifurcation or imperfection sensitivity of the structure.

Substituting Eq. (11) into Eq. (10) and collecting terms of the same power of ξ, an ordered set of perturbation equations result:

$$H_{ij}L_{1_{ik}}(u_k^{(1)})\cdot L_{1_{jl}}(\delta u_l) + \sigma_i^0\cdot L_{11_i}(u_l^{(1)}, \delta u_l) = 0 \tag{12a}$$

$$H_{ij}L_{1_{ik}}(u_k^{(2)})\cdot L_{1_{jl}}(\delta u_l) + \sigma_i^0\cdot L_{11_i}(u_l^{(2)}, \delta u_l) + \tfrac{1}{2}H_{ij}L_{2_{ik}}(u_k^{(1)})\cdot L_{1_{jl}}(\delta u_l) + H_{ij}L_{1_{ik}}(u_k^{(1)})\cdot L_{11_i}(u_l^{(1)}, \delta u_l) = 0 \tag{12b}$$

Here we show only the first- and second-order equations. The first-order equation constitutes an eigenvalue problem that on solution yields the buckling load and the mode. These are the necessary input for treating the second-order equation. In the asymptotic approach,[10] the total deformation is considered to be made up of two parts, viz., the buckling mode controlled by a scaling factor plus additional modes of deformation that are orthogonal to it. The former is obtained by the solution of the first-order equation and the latter, which is in the nature of a modification to the former, is obtained by the consideration of second-order and, if necessary, higher order equations. Thus an orthogonality condition between $u^{(1)}$ and $u^{(2)}$ that are the solution vectors of the first-order and second-order equations, respectively, must be imposed.[10] This orthogonality condition will be seen to be automatically satisfied in the present work by the choice of the displacement functions of the first- and second-order displacement fields.

Buckling Problem

From Eq. (12a) a potential energy function for the first-order field problem can be set up in the following form:

$$\Pi^{(1)} = \tfrac{1}{2}\{H_{ij}L_{1_{ik}}(u_k^{(1)})\cdot L_{1_{jl}}(u_l^{(1)}) + \sigma_i^0\cdot L_{2_{ik}}(u_k^{(1)})\} \tag{13}$$

In a manner shown in Ref. 7, it can be shown for a stiffened shell built up of specially orthotropic laminates the displacement functions that satisfy the governing differential equations are of the following form:

$$u = u_i\phi_i(y)\cos\left(\frac{m\pi x}{L}\right) \tag{14a}$$

$$\alpha = \alpha_i\phi_i(y)\cos\left(\frac{m\pi x}{L}\right) \tag{14b}$$

$$v = v_i\phi_i(y)\sin\left(\frac{m\pi x}{L}\right) \tag{14c}$$

$$w = w_i\phi_i(y)\sin\left(\frac{m\pi x}{L}\right) \tag{14d}$$

$$\beta = \beta_i\phi_i(y)\sin\left(\frac{m\pi x}{L}\right) \tag{14e}$$

where u_i, v_i, . . . , etc., are the degrees of freedom (DOFs), and the ϕ_i are appropriately chosen polynomial functions. In the present work, the functions ϕ_i are chosen in the hierarchical form in the manner advocated by Szabo and Babuska.[14] These are obtainable by integration of the Legendre functions and provide automatically for C_0 continuity. Thus, these are convenient to use in SDT formulation and are available in Ref. 14. Several computations were performed using the standard Lagrange polynomials as well. These have the merit of being able to display readily the buckling mode over the interior regions of an element without further calculations. For the CPT formulation, Hermitian cubic polynomials are used for w and linear functions for u and v.

Designating the DOFs of the buckling problem as $q_i^{(1)}$, the potential energy function governing the buckling problem may be expressed as

$$\Pi^{(1)} = \tfrac{1}{2}[a_{ij}^{(1)} - \lambda b_{ij}^{(1)}]q_i^{(1)}q_j^{(1)} \qquad (i, j = 1, 2, \ldots, n_1) \tag{15}$$

where n_1 is the number of DOFs employed in the discretization. The equations of equilibrium follow:

$$[a_{ij}^{(1)} - \lambda b_{ij}^{(1)}]q_j^{(1)} = 0 \qquad (i, j = 1, 2, \ldots, n_1) \tag{16}$$

Equation (16) constitutes the familiar eigenvalue problem for λ_c (the eigenvalue) and $q_i^{(1)}$ (the eigenmode).

Second-Order Field Problem

From the variational equation of equilibrium [Eq. (12b)], a potential energy function for the second-order field problem can be constructed and takes the form

$$\Pi^{(2)} = \tfrac{1}{2}[H_{ij}L_{1_{ik}}(u_k^{(2)})\cdot L_{1_{jl}}(u_l^{(2)}) + \sigma_i^0\cdot L_{2_{ik}}(u_k^{(2)}) + H_{ij}\{L_{2_{ik}}(u_k^{(1)})\cdot L_{1_{jl}}(u_l^{(2)}) + 2L_{1_{ik}}(u_k^{(1)})\cdot L_{11_{jl}}(u_l^{(1)}, u_l^{(2)})\}] \tag{17}$$

Displacement Functions

To determine the x variation of the displacements, we proceed in the manner outlined in Ref. 12. For the case of shell structure built up of specially orthotropic material and subjected to prescribed end compression, the solution takes the following form:

$$u^{(2)} = u_{2_i}^{(2)}\phi_i(y)\sin\left(\frac{2m\pi x}{L}\right) \tag{18a}$$

$$\alpha^{(2)} = \alpha_{2_i}^{(2)}\phi_i(y)\sin\left(\frac{2m\pi x}{L}\right) \tag{18b}$$

$$v^{(2)} = v_{0_i}^{(2)}\phi_i(y) + v_{2_i}^{(2)}\phi_i(y)\cos\left(\frac{2m\pi x}{L}\right) \tag{18c}$$

$$w^{(2)} = w_{0_i}^{(2)}\phi_i(y) + w_{2_i}^{(2)}\phi_i(y)\cos\left(\frac{2m\pi x}{L}\right) \tag{18d}$$

$$\beta^{(2)} = \beta_{0_i}^{(2)}\phi_i(y) + \beta_{2_i}^{(2)}\phi_i(y)\cos\left(\frac{2m\pi x}{L}\right) \tag{18e}$$

The y variation of the displacements $[\phi_i(y)]$ are chosen to be the same type as in the eigenvalue problem.

Degree of Freedom of the Second-Order Problem

Note that the displacement functions contain two components: one that is independent of x and the other that depicts a harmonic variation in the x direction of half the wavelength of the buckling mode. Thus there are two sets of DOFs: set 1, associated with the former, and set 2, associated with the latter. Thus the total number of DOFs (n_2) is greater than in the buckling problem, but the DOFs of set 1 decouple from set 2 in the solution process, and hence they can be determined independently of each other. It should also be noted that, in solving for the DOFs of set 1, at least three boundary constraints must be specified to eliminate rigid-body translations and rotations. Note that, irrespective of the symmetry or antisymmetry of the buckling mode with respect to the centerline of the panel, the second-order field would always be symmetric. Further, to model a panel that is part of a shell structure, the centerline is allowed to move in the transverse direction while constraining it to remain straight.

Solution Procedure

The potential energy function [Eq. (17)] can now be expressed in terms of the degrees of freedom $q_r^{(1)}$ and $q_i^{(2)}$ defining the first- and second-order fields, respectively. This takes the following form:

$$\Pi^{(2)} = \tfrac{1}{2}[a_{ij}^{(2)} - \lambda b_{ij}^{(2)}]q_i^{(2)}q_j^{(2)} + c_{irs}q_i^{(2)}q_r^{(1)}q_s^{(1)}$$

$$(r, s = 1, \ldots, n_1 \qquad i, j = 1, 2, \ldots, n_2) \tag{19}$$

The equations of equilibrium take the following form:

$$[a_{ij}^{(2)} - \lambda b_{ij}^{(2)}]q_j^{(2)} = -c_{irs}q_r^{(1)}q_s^{(1)} \tag{20}$$

where λ is set equal to λ_{cr} in the solution of Eq. (20).

Determination of the Postbuckling Response

With the first- and second-order fields computed, it is possible to express the displacement field of the structure in terms of a single variable ξ using Eq. (11). A potential energy function for the buckled structure is thus set up in terms of a single variable ξ. This takes the form

$$\Pi = (\bar{a} - \lambda\bar{b})\xi^2 + \bar{c}\xi^3 + \bar{d}\xi^4 \tag{21}$$

where

$$\bar{a} = \tfrac{1}{2}a_{ij}^{(1)}q_i^{(1)}q_j^{(1)} \qquad \bar{b} = \tfrac{1}{2}b_{ij}^{(1)}q_i^{(1)}q_j^{(1)}$$

and $\bar{c}$ and $\bar{d}$ can be expressed as

$$\bar{c} = \tfrac{1}{2}H_{ij}L_{1_{ik}}(u_k^{(1)}) \cdot L_{2_{jl}}(u_l^{(1)}) = e_{ijk}q_i^{(1)}q_j^{(1)}q_k^{(1)} \tag{22a}$$

$$\bar{d} = \tfrac{1}{2}H_{ij}\{\tfrac{1}{2}L_{2_{ik}}(u_k^{(1)}) \cdot L_{1_{jr}}(u_r^{(2)}) + L_{1_{ik}}(u_k^{(1)}) \cdot L_{11_{jr}}(u_l^{(1)}, u_r^{(2)}) + \tfrac{1}{4}L_{2_{ik}}(u_k^{(1)}) \cdot L_{2_{jl}}(u_l^{(1)})\}$$

$$= f_{rjk}q_r^{(2)}q_j^{(1)}q_k^{(1)} + g_{ijkl}q_i^{(1)}q_j^{(1)}q_k^{(1)}q_l^{(1)}$$

$$(i, j, k, l = 1, \ldots, n_1; \qquad r = 1, \ldots, n_2) \tag{22b}$$

For shell structures that are sufficiently long (say, $m > 8$), m may always be deemed to be even and as a result $\bar{c} = 0$ and the bifurcation is symmetric. The equilibrium path giving the postbuckling response takes the form

$$\lambda = \lambda_{cr} + \lambda_2\xi^2 \tag{23}$$

where $\lambda_{cr} = \bar{a}/\bar{b}$, and $\lambda_2 = 2\bar{d}/\bar{b}$. This equation relates the amplitude of the local buckles to the end shortening.

Postbuckling Stiffness and Imperfection Sensitivity

The tangent stiffness of the structure is given by $dF/d\Delta$, the rate of change of F, the total axial force (F) carried by the structure to the total end-shortening (Δ). Equivalently, this can be expressed as $d\sigma_{av}/d\lambda$, where σ_{av} is the average stress carried by the entire section of the panel and can be written as

$$\sigma_{av} = \sigma_{cr} + \sigma_2^{ef}\xi^2 \tag{24}$$

where σ_{cr} and σ_2^{ef} are, respectively, the averaged critical stress and the second-order component of the averaged axial stress. Note that all of the three σ (viz., σ_{av}, σ_{cr}, and σ_2^{ef}) are taken as positive when compressive. The last is made up of two contributions:

$$\sigma_2^{ef} = E_x\lambda_2 - \sigma_2 \tag{25}$$

where E_x is the averaged longitudinal modulus, which is also the stiffness of the unbuckled structure, and σ_2 is the averaged longitudinal stress contributed by the second-order field (taken as positive when tensile). The postbuckling stiffness E_x^* and the ratio of the postbuckling stiffness to the prebuckling stiffness r take the forms

$$E_x^* = \frac{\sigma_2^{ef}}{\lambda_2}, \qquad r = \frac{E_x^*}{E_x} = \frac{\sigma_2^{ef}}{E_x\lambda_2} \tag{26}$$

To assess the imperfection sensitivity, Eq. (24) is rewritten in the form

$$\frac{\sigma_{av}}{\sigma_{cr}} = 1 + b^*\xi^2 \tag{27}$$

where $b^* = \sigma_2^{ef}/\sigma_{cr}$. If b^* is negative, the structure is imperfection sensitive, and if b^* is positive, the structure has a positive postbuckling load-carrying capacity. If $\bar{\xi}$ is the scaling parameter of an imperfection in the form of the buckling mode, then the maximum load can be approximated by

$$\frac{\sigma_{max}}{\sigma_{cr}} = 1 - 3(-b^*)^{(1/3)}\left(\frac{\bar{\xi}}{2}\right)^{(2/3)} \tag{28}$$

The value of b^* depends on how the buckling mode is normalized. In all of the computations, the buckling mode was expressed taking the maximum normal deflection in the structure to be unity.

Results and Discussion

In this section numerical results of isolated panels and stiffened panels are presented and discussed. Two types of material are considered, viz., isotropic and layered specially orthotropic. Both CPT and SDT are used with a view to assessing the influence of shear deformation. Numerical results from CPT are obtained using h-version finite strips with hermitian cubics for out-of-plane displacements and linear interpolating functions for the in-plane displacements. For SDT, p-version Legendre (or Lagrange) polynomials are used, with a relatively high value of $p(\geq 5)$ and a small number of strips. This provides a comparison between the rates of convergence of the two numerical approaches. For the layered material, which consisted of eight layers of equal thickness, the following properties were assumed: Lay-up sequence $\{0/90/0/90\}_s$;

$E_1/E_2 = 18.28$, $E_1/G_{12} = 37.39$, $\nu_{12} = 0.24$, $G_{12} = G_{23} = G_{31}$. (Compare with $E_1 = 32900$ ksi, $E_2 = 1800$ ksi, $G_{12} = 880$ ksi, and $\nu_{12} = 0.24$ for typical glass epoxy.) Poisson's ratio for the isotropic material ν is assumed to be 0.3.

The results of the computation were checked against standard and well-known results available in the literature on the buckling and postbuckling analysis of plates and shells.[1,9,15] In addition, the SDT program was checked in all of the cases by setting the transverse shear modulus to an arbitrarily high value and thus recovering the CPT results.

Isolated Panels

As a first example we present the results for an isolated panel simply supported along its longitudinal edges and subjected to uniform end-shortening. The geometry is defined by $R/t = 200$ and $b/t = 50$. The symmetry of deformation is imposed with respect to the middle of the panel, whereas the edges of the panel are assumed to be simply supported ($w = 0$) but otherwise free. Absence of longitudinal shear along the edges insures that the total force carried by the panel at any section must be the same, thus providing an equilibrium check for the results. As a first step, the half-wavelength that corresponds to the minimum critical load is determined in each case.

Convergence of the Solution

The results of a convergence study are presented in Tables 1 and 2 for CPT and SDT, respectively. The convergence for the critical loads in all of the cases is rapid and presents no problems. However, it is evident that p-version based SDT has a much faster rate of convergence than the h-version based CPT. Postbuckling behavior is characterized by $\bar{\sigma}_2 (= \sigma_2^{ef}/E_x)$ and λ_2 or b^* and r. Although for isotropic panels, the h-version based CPT does produce satisfactory results, say with 24 strips, difficulties arise for the case of orthotropic material. Convergence in this case is slow and requires a large number of DOFs for usual tolerances acceptable for numerical work (say 0.1%). This is essentially attributable to the choice of linear shape functions to describe u and v in the CPT formulation. On the other hand, p-version based SDT produces a rapid convergence with a relatively small number of DOFs . In this case, p-level was kept fixed at 5 and the number of strips was increased from 1 (30 DOF) to 3 (80 DOF). All of the key indicators of postbuckling behavior were predicted with sufficient accuracy with just one strip for both the materials.

Isotropic vs Composite Panels

The composite shell panel has a much lower critical load as compared with that of the isotropic panel, which appears to be primarily attributable to the low Q_{12}/Q_{11} and Q_{66}/Q_{11} of the basic material reflecting in relatively poor values of A_{12}/A_{11}, A_{66}/A_{11}, D_{12}/D_{11}, and D_{66}/D_{11} in comparison with those of the isotropic material. (However, notice that, for the panels of the type studied here, the wavelengths of buckling are substantially the same.) It is interesting to see that the composite panel has a stable postbuckling response, whereas the isotropic panel turns out to be highly imperfection sensitive. In fact, the relationship between the load sustained and end-shortening is strongly re-entrant for the isotropic panel with $R/t = 200$ indicating severe imperfection sensitivity and snap-through buckling under controlled end-shortening. The explanation for this behavior may be sought in terms of the high membrane energy stored in the prebuckling stage and its sudden dissipation at the onset of buckling as given by $L_1(u^{(1)}) \cdot L_{11}(u^{(2)}, u^{(1)})$ terms, i.e., primarily by the modification of the buckling deformation as given by the second-order field. In contrast, the composite panel does not store a high level of membrane energy as indicated by the relatively low buckling load, and in this respect its behavior approaches that of a plate.

On the whole, for the b/t and R/t selected, it appears that the effect of shear deformation is minimal, both with regard to the critical load as well as the half-wavelength of buckling. For the composite material for which the transverse shear moduli (herein assumed to be the same in magnitude as G_{12}) are a small fraction of E_{11}, the effect is somewhat noticeable with about a 16% drop in the value of r accounted for by shear deformation. Since the postbuckled stiffness is very small for the panel in this case, this drop is not significant for practical purposes.

Behavior as R/t Varies

The key factors that control the postbuckling response of an isolated panel are the R/t and b/t ratios. For isotropic panels, Koiter[1] introduced a single parameter, the so-called "flatness parameter" θ, which he showed to be an adequate index of the postbuckling response. This parameter encapsulates within itself both b/t and R/t and can be expressed thus:

$$\theta = \frac{1}{2\pi}[12(1-\nu^2)]^{1/4}\left(\frac{b}{\sqrt{Rt}}\right) \tag{29}$$

Table 1 Convergence study on isolated panels: CPT results

Material	No. of Elements	No. of DOF	$\sigma_{cr}/E_x \times 10^4$	$\bar{\sigma}_2 \times 10^4$	$\lambda_2 \times 10^4$	b^*	r[a]
Isotropic	12	52	20.829	−9.838	−6.720	−0.472	1.464
$\ell/t = 63.0$	24	100	20.664	−9.878	−6.760	−0.478	1.461
	36	148	20.633	−9.889	−6.772	−0.479	1.461
Orthotropic	12	48	9.095	0.589	3.802	0.0647	0.155
$\ell/t = 62.0$	24	100	8.988	0.473	3.687	0.0526	0.128
	36	148	8.968	0.450	3.664	0.0502	0.123
	50	204	8.960	0.441	3.655	0.0492	0.121

[a]A value of r in Tables 1-5 numerically greater than unity indicates a re-entrant postbuckling path.

Table 2 Convergence study on isolated panels: SDT results

Material	No. of Elements	No. of DOF	$\sigma_{cr}/E_x \times 10^4$	$\bar{\sigma}_2 \times 10^4$	$\lambda_2 \times 10^4$	b^*	r
Isotropic	1	30	20.579	−9.9074	−6.8864	−0.4814	1.4387
$\ell/t = 64.0$	2	55	20.579	−9.9075	−6.8865	−0.4814	1.4387
	3	80	20.579	−9.9075	−6.8865	−0.4814	1.4387
Orthotropic	1	30	8.9053	0.3633	3.5775	0.04080	0.1016
$\ell/t = 62.0$	2	55	8.9052	0.3634	3.5776	0.04081	0.1016
	3	80	8.9052	0.3634	3.5778	0.04081	0.1016

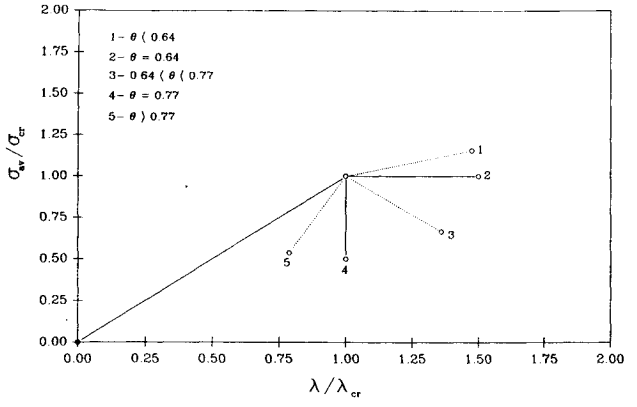

Fig. 2 Nondimensional load vs end-shortening relationships of Koiter panels.

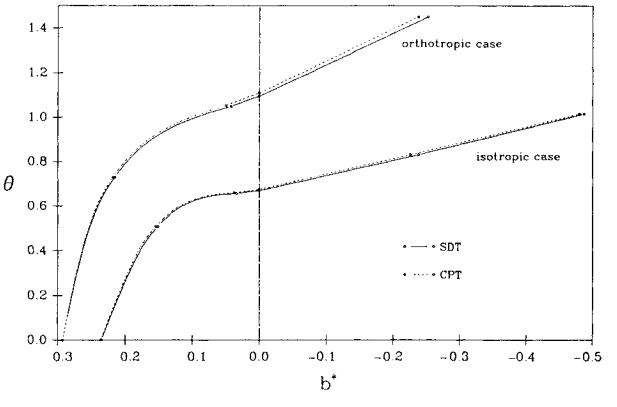

Fig. 3 Imperfection sensitivity of isolated panels.

Table 3 Convergence study on stiffened panels: CPT results

Material	No. of Elements	No. of DOF	σ_{cr}/E_x $\times 10^4$	$\bar{\sigma}_2$ $\times 10^4$	λ_2 $\times 10^4$	b^*	r
Isotropic $\ell/t = 31.5$	32 (12 + 12 + 8)	132	35.525	−14.612	−7.661	−0.411	1.907
	60 (24 + 24 + 12)	244	35.513	−14.742	−7.793	−0.415	1.892
	75 (30 + 30 + 15)	304	35.513	−14.755	−7.807	−0.415	1.890
	100 (40 + 40 + 20)	404	35.511	−14.769	−7.820	−0.416	1.888
Orthotropic $\ell/t = 75.5$	32 (12 + 12 + 8)	132	11.881	0.2219	2.071	0.0187	0.1072
	60 (24 + 24 + 12)	244	11.773	0.2034	2.049	0.0173	0.0993
	75 (30 + 30 + 15)	304	11.762	0.2014	2.047	0.0171	0.0984
	100 (40 + 40 + 20)	404	11.751	0.1995	2.044	0.0170	0.0976

Under prescribed compressive loading, the postbuckling equilibrium of a simply supported panel is unstable for $\theta > 0.64$, and the severity of imperfection sensitivity increases with θ. For $\theta < 0.64$, the panel ceases to be imperfection sensitive (for local buckling) and, as R/t increases, behaves more and more like a plate panel. Figure 2 shows qualitatively how a nondimensional load end-shortening relationship will look for various values of θ.

Figure 3 shows the variation of b^* with θ for isotropic and composite panels, respectively. In all of these cases, b/t is kept fixed at 50, where R/t was varied to produce panels of varying flatness. In each case the values as given by both CPT and SDT are plotted. It is evident that the differences are not appreciable. For the isotropic case, b^* goes through zero at about $\theta = 0.67$, which differs from Koiter's value of 0.64. The reasons for this discrepancy are not hard to find. It stems from the difference in the boundary conditions along the longitudinal edges along which $u = 0$ in Koiter's analysis, whereas it is free in our case. Yet another point of minor difference is that we solve a case of prescribed compression, whereas Koiter solves the case of prescribed uniform stress.

A comparison of the characteristics plotted in Fig. 3 reveals a striking contrast in the behavior of the two types of panels. The composite panel shows little imperfection sensitivity for a wide range of practical values of θ. Note that the expression for θ is strictly not applicable for the composite panel, but we nevertheless regard it as a useful parameter with ν_{12} replacing ν in Eq. (29). The b^* remains positive for values of $\theta < 1.1$. Thus, the composite panels of the type studied here buckle under a significantly smaller nondimensional load but have markedly less imperfection sensitivity than isotropic panels of the same geometry.

Stiffened Panels

In this section we present results that illustrate the behavior of stiffened panels. We consider panels with $b/t = 50$ (b is the stiffener spacing) with R/t assuming values ∞, 200, and 50, respectively. As before, the panel is assumed to be fabricated out of either isotropic or layered specially orthotropic material. The material properties are the same as for the case of isolated panels discussed in the previous section. The stiffeners are rectangular outstands with $d_s/t = 15$ and 10 and with $t_s/t = 2$. The lay-up sequence for the stiffener is the same as that for the shell.

Convergence of Numerical Solution

Tables 3 and 4 summarize the results of both the buckling and postbuckling analyses as given by CPT and SDT, respectively. The convergence of the CPT solution is monotonic as can be seen from the results displayed in Table 3. The apportioning of the total number of strips between the shell and stiffener is indicated in column 2, where for example the arrangement (12 + 12 + 8) indicates 12 strips in each half of the shell panel and 8 strips in stiffener.

The convergence of the SDT results (Table 4) is examined with respect to the number of strips (n) and the polynomial degree (p) of the displacement functions. In this case the convergence is somewhat slower than in the corresponding isolated panel case. This is believed to be due to the shear deformation associated with the stiffener and the fact that our model is in a strict sense nonconforming because of the unmatched rotational degrees of freedom at the stiffener and shell junction. It is interesting to observe that, as p increases through 4, 5, and 8 (with n remaining the same), the model exhibits a slight increase in the postbuckling stiffness. This

appears to be a deviation from the general pattern of convergence in displacement approach where the stiffness must decrease with increasing numbers of degrees of freedom. It is apparent that the convergence is in fact oscillatory as can be verified by taking $p = 3$ (the result not shown) so that in the range of p considered it approaches the exact value from below. This kind of oscillatory convergence is a characteristic of nonconforming finite element models. In the results presented in Table 4, this effect is seen in both isotropic and orthotropic panels. Table 4 also gives the results for $p = 5$ and the strip configuration given by (2 + 2 + 1). It is seen that no significant improvement in the accuracy of the critical load or the postbuckling stiffness is achieved by increasing the number of strips.

Salient Features of Structural Response

The load end-shortening response of panels ($\bar{\sigma}$ vs λ relationships) as obtained, respectively, by CPT and SDT are given in Figs. 4–7. Table 5 summarizes the essential results in dimensionless forms of the family of panels investigated. The CPT results were produced using 75 strips (30 + 30 + 15), and the SDT results were produced taking $n = 3$ and $p = 5$. The results are discussed in the sequel.

Effect of Shear Deformation

Isotropic panels: The effect of shear deformation on the buckling load and the postbuckling response on stiffened panels appears to be marginal despite the relatively stocky stiffeners considered in the example. (Refer to Figs. 4a, 5a, and 6a.)

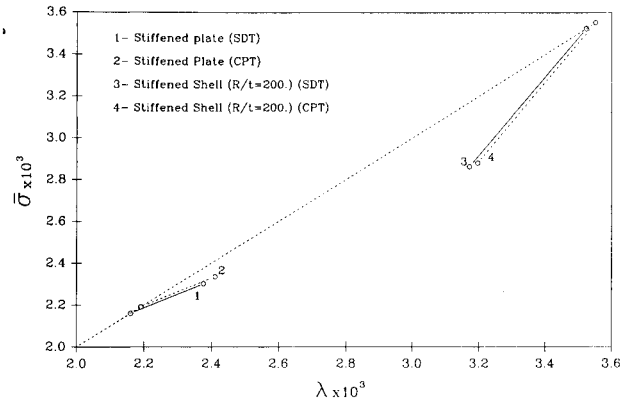

Fig. 4a Load vs end-shortening characteristics of isotropic stiffened panels ($d_s/t = 15$).

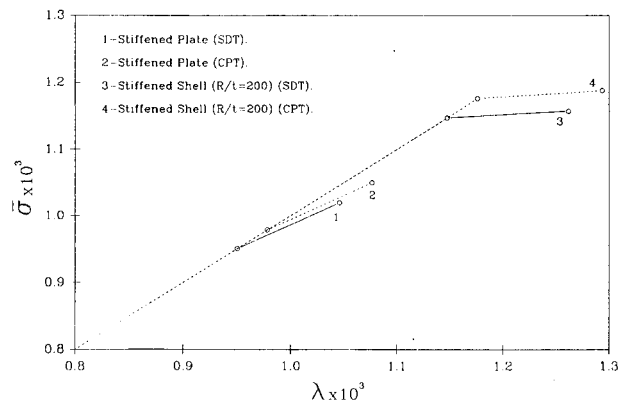

Fig. 4b Load vs end-shortening characteristics of orthotropic stiffened panels ($d_s/t = 15$).

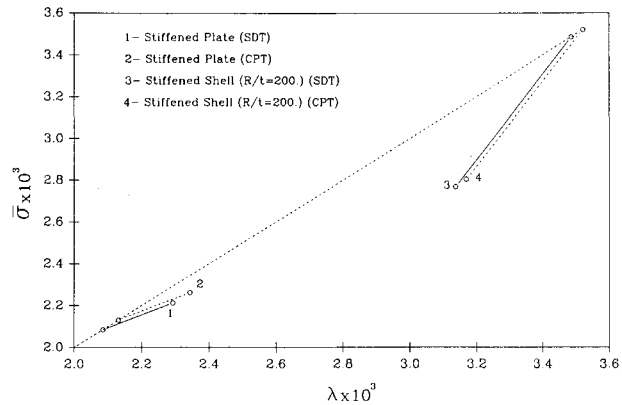

Fig. 5a Load vs end-shortening characteristics of isotropic stiffened panels ($d_s/t = 10$).

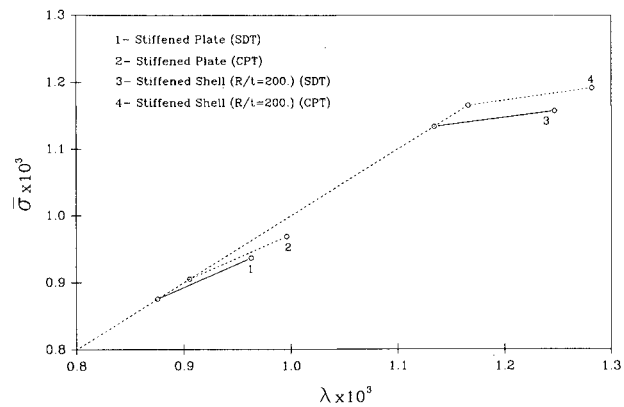

Fig. 5b Load vs end-shortening characteristics of orthotropic stiffened panels ($d_s/t = 10$).

Table 4 Convergence study on stiffened panels: SDT results

Material	n and p	No. of DOF	σ_{cr}/E_X $\times 10^4$	$\bar{\sigma}_2$ $\times 10^4$	λ_2 $\times 10^4$	b^*	r
Isotropic $\ell/t = 31.5$	$n = 3$ $p = 4$	66	35.278	−14.732	−7.739	−0.418	1.904
	$n = 3$ $p = 5$	81	35.238	−15.006	−8.008	−0.426	1.874
	$n = 5$ $p = 5$	131	35.237	−15.027	−8.028	−0.426	1.872
	$n = 3$ $p = 8$	126	35.227	−15.027	−8.024	−0.427	1.873
Orthotropic $\ell/t = 75.5$	$n = 3$ $p = 4$	66	11.514	0.175	2.027	0.0152	0.0865
	$n = 3$ $p = 5$	81	11.472	0.181	2.037	0.0158	0.0891
	$n = 5$ $p = 5$	131	11.472	0.181	2.037	0.0158	0.0898
	$n = 3$ $p = 8$	126	11.463	0.183	2.039	0.0159	0.0897

Table 5 Summary of response of stiffened panels

	$d_s/t = 15$, $t_s/t = 2$				$d_s/t = 10$, $t_s/t = 2$				
R/t	ℓ/t	$\lambda_{cr} \times 10^2$	b^*	r	ℓ/t	$\lambda_{cr} \times 10^2$	b^*	r	Theory
Isotropic panels									
∞ (plate	40.0	0.216	0.385	0.654	41.5	0.208	0.358	0.614	SDT
panels)	39.5	0.219	0.390	0.657	40.5	0.213	0.366	0.616	CPT
200	31.5	0.352	−0.426	1.874	32.0	0.349	−0.478	1.870	SDT
	31.5	0.355	−0.415	1.890	31.5	0.352	−0.442	2.037	CPT
50	13.0	1.213	−0.804	1.663	13.0	1.212	−0.848	1.766	SDT
	13.0	1.225	−0.771	1.696	13.0	1.224	−0.815	1.804	CPT
	51.0[a]	0.826	0.0236	0.519	—	—	—	—	SDT
Composite stiffened panels									
∞ (plate	68.5	0.0951	0.543	0.723	62.0	0.080	0.636	0.700	SDT
panels)	69.0	0.0979	0.531	0.728	62.0	0.091	0.618	0.702	CPT
200	75.5	0.115	0.016	0.089	65.5	0.113	0.057	0.212	SDT
	75.5	0.118	0.017	0.098	65.5	0.117	0.055	0.223	CPT
50	96.5	0.285	0.005	0.064	101.0	0.385	−0.048	3.195	SDT
	94.5	0.292	0.008	0.094	95.0	0.393	−0.049	3.928	CPT

[a]Antisymmetric "stiffener" mode.

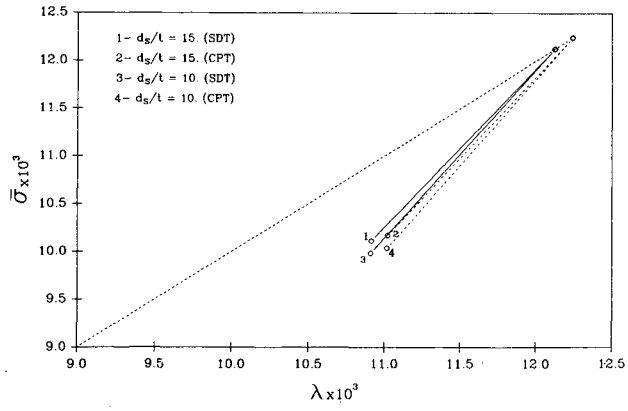

Fig. 6a Load vs end-shortening characteristics of isotropic stiffened panels ($R/t = 50$).

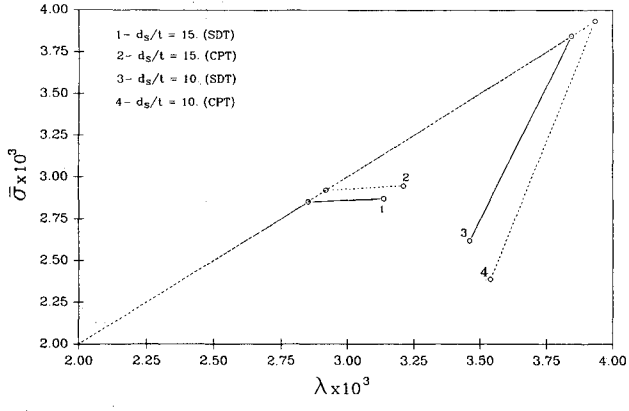

Fig. 6b Load vs end-shortening characteristics of orthotropic stiffened panels ($R/t = 50$).

Plate panels ($R/t = \infty$) (Figs. 4a and 5a): A comparison of the critical loads as given by the two theories indicates that shear deformation accounts for a small, but noticeable, reduction in the critical stress, and this reduction appears to stem mainly from the action of the relatively stocky stiffener. But the postbuckling stiffness as given by r is not affected to any noticeable extent. Any discrepancy in this is due to the change in wavelength of buckling when shear deformation is considered and does not come from the second-order field, which involves little out-of-plane action.

Panels with $R/t = 200$ (Figs. 4a and 5a): The reduction in buckling stress in this case is even less noticeable than in plate

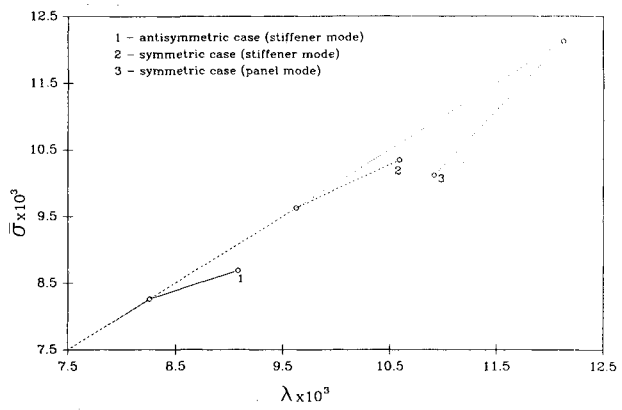

Fig. 7 Load vs end-shortening characteristics for symmetric and antisymmetric modes.

panels, since the effect of curvature tends to dominate over that of shear deformation. Postbuckling characteristics predicted by SDT are more sharply re-entrant than those given by CPT. The values of b^* obtained are consistent with this observation, i.e., SDT predicts a greater imperfection sensitivity as it gives a smaller (negative, but numerically higher) value of b^* in both the cases investigated.

Panels with $R/t = 50$ (Figs. 6a, 7, and 8): The CPT once again underestimates the imperfection sensitivity, as seen from the values of b^* in Table 5. However, values of the critical stresses are little affected by shear deformation because it is overshadowed by the effect of curvature. Both the panels exhibit severe imperfection sensitivity and sharply re-entrant postbuckling characteristics.

The panel with $d_s/t = 15$ has two competing modes, one antisymmetric and the other symmetric with respect to the center of the panel. These are "stiffener modes," and the former is sketched in Fig. 8 along with the "panel" mode, which is symmetric with respect to the center of the panel. The panel mode is associated with a higher buckling load ($\lambda_{cr} = 0.0121$) but exhibits an unstable postbuckling response. In contrast, the stiffener modes, which are associated with lower buckling loads (e.g., $\lambda_{cr} = 0.00826$, for the lower antisymmetric stiffener mode), give a stable postbuckling response. The results for this case as given by SDT are included in Table 5. These modes are associated with considerable bending of the stiffener in comparison with the panel mode. The wavelength of the panel mode is far smaller ($\ell/t = 13$) than that of the stiffener mode ($\ell/t = 51$). In Fig. 6a we have shown the responses associated with the higher unstable

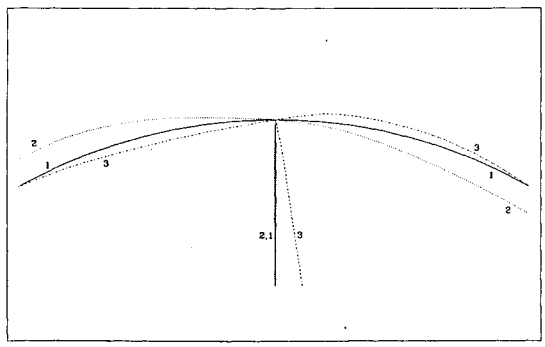

Fig. 8 Governing modes of isotropic stiffened panels ($R/t = 50$, $d_s/t = 15$).

modes, being perhaps more critical from the point of view of actual shell behavior. However, one would expect the shell to first buckle in the lower stable mode and then go through an unstable bifurcation in sympathy with the higher mode or be subject to some interaction between all of the three modes in the presence of imperfections. The individual responses of the three modes are shown in Fig. 7. Interestingly, for the case with $d_s/t = 10$, the stiffener modes are associated with critical loads which are higher than those for the unstable panel mode and hence are not of any interest. Note, however, the panel with $R/t = 50$ is not indeed shallow enough for Donnel's theory to be sufficiently accurate.

Orthotropic panels: For stiffened panels fabricated out of layered orthotropic material, the effect of shear deformation is far greater than that observed in the case of isotropic panels.

Plate panels (Figs. 4b and 5b): In this case, CPT overestimates the critical load by margins more significant than those seen in the case of isotropic panels. In the case with $d_s/t = 10$, the error involved in the CPT prediction of the critical stress is about 14% (with respect to SDT prediction) in contrast to 2% seen in the case of isotropic panels. However, as in the case of unstiffened plates discussed earlier, the stiffness ratio r is not noticeably affected.

Panels with $R/t = 200$ (Figs. 4b and 5b): CPT overestimates the critical loads by less significant margins, as seen earlier for isotropic panels. With regard to postbuckling behavior, the panels exhibit stable postbuckling response. The value of r, as given by CPT, exceeds that given by SDT by at least 5%. Thus, CPT overestimates not only the critical load but also the postbuckling stiffness.

Panels with $R/t = 50$ (Fig. 6b): Again, the discrepancies between the two theories in the predictions of the buckling loads are relatively minor, with CPT overestimating the critical load by about 2-3%. The panel with $d_s/t = 15$ gives a stable postbuckling response, since the buckling is initiated by the stiffener. In this case, CPT overestimates the postbuckling stiffness by a noticeable margin. However, since the postbuckling stiffness is close to zero in either case, the discrepancy has little practical significance. In contrast, for the panel with $d_s/t = 10$, both the theories give unstable postbuckling paths, with CPT giving a somewhat reduced imperfection sensitivity.

Composite vs Isotropic Panels

As in the case of isolated panels discussed earlier, the composite panels show significantly reduced critical stresses as measured by λ_{cr}. Again, the postbuckling stiffnesses of the composite panels are significantly higher (or, alternatively, the imperfection sensitivities are much smaller) than the corresponding isotropic panels for all of the cases studied here. This means that the buckling loads can be better predicted for composite panels, and thus the composites offer themselves as more robust materials for structural engineering purposes.

Conclusion

Local postbuckling of composite and isotropic shell panels was studied using both Kirchhoff and Reissner-Mindlin plate theories (designated as CPT and SDT, respectively). Numerical analyses were performed using p-version based SDT and h-version based CPT finite strips. Detailed convergence studies are reported. Studies confirm the efficacy of the p-version approach as demonstrated by a rapid convergence of the key results. Shear deformation effects are much more important in stiffened composite shell problems than in isolated panels and must be included for accurate predictions. Shallow orthotropic layered stiffened shells studied here ($R/t = 200$) had a much lower nondimensional critical load than the corresponding isotropic panels but exhibited positive postbuckling stiffnesses in contrast to isotropic panels that were found to be very imperfection sensitive. CPT overestimates the critical loads in all cases, but the error is small for the panel geometries studied here. With regard to postbuckling behavior, CPT overestimates the postbuckling stiffnesses for composite panels and underestimates the imperfection sensitivity of isotropic shell panels. Panels having relatively slender stiffeners may buckle in "stiffener buckling" mode, but this mode produces a stable postbuckling response; in such cases a higher panel mode may, in fact, govern the shell behavior.

Acknowledgment

Support for this research was provided in part by the NASA Langley Research Center under Grant NAG-1-1279.

References

[1]Koiter, W. T., "Buckling and Postbuckling Behavior of a Cylindrical Panel Under Axial Compression," National Aeronautical Research Inst., Rept. S.476, Amsterdam, 1956.

[2]Singer, J., and Haftka, R., "Buckling of Discretely Stringer-Stiffened Cylindrical Shells Under Axial Compression," Technion, TAE Rept. 91, Haifa, Israel, 1974.

[3]Stephens, W. B., "Imperfection-Sensitivity of Axially Compressed Stringer-Reinforced Cylindrical Panels Under Internal Pressure," *AIAA Journal,* Vol. 9, No. 9, 1971, pp. 1713-1719.

[4]Wang, J. T. S., and Lin, Y. J., "Stability of Discretely Stringer-Stiffened Cylindrical Shells," *AIAA Journal,* Vol. 11, No. 6, 1973, pp. 810-814.

[5]Syngellakis, S., and Walker, A. C., "Elastic Buckling of Cylinders with Widely Spaced Stiffeners," *Proceedings of the Third IUTAM Symposium on Shell Theory* (Tbilisi), edited by W. T. Koiter and G. K. Mikhailov, North-Holland, Amsterdam, 1978, pp. 553-574.

[6]Hui, D., and Chen, Y. H., "Imperfection-Sensitivity of Cylindrical Panels Under Compression Using Koiter's Improved Theory," *International Journal of Solids and Structures,* Vol. 23, No. 7, 1987, pp. 969-982.

[7]Kapania, R., "A Review of the Analysis of Laminated Shells," *ASME Journal of Pressure Vessel Technology,* Vol. 111, No. 2, 1989, pp. 88-96.

[8]Zeggane, M., and Sridharan, S., "Buckling Under Combined Loading of Shear Deformable Laminated Anisotropic Plates Using 'Infinite' Strips," *International Journal of Numerical Methods in Engineering,* Vol. 31, No. 7, 1991, pp. 1319-1331.

[9]Zeggane, M., and Sridharan, S., "Stability Analysis of Long Laminated Composite Plates Using Reissner-Mindlin 'Infinite' Strips," *Computers and Structures,* Vol. 40, No. 1, 1991, pp. 1033-1042.

[10]Budiansky, B., "Dynamic Buckling of Elastic Structures: Criteria and Estimates," *Dynamic Stability of Structures,* edited by G. Herrman, Pergamon Press, Oxford, England, UK, 1966, pp. 83-106.

[11]Bushnell, D., *Computerized Buckling Analysis of Shells,* 1st ed., Martinus Nijhoff Publishers, Dordrecht, The Netherlands, 1985, pp. 272-277.

[12]Jones, R. M., *Mechanics of Deformable Bodies,* Hemisphere, New York, 1975, pp. 152-156.

[13]Brush, D. O., and Almroth, B. O., *Buckling of Bars, Plates and Shells,* McGraw-Hill, New York, 1975, pp. 143-148.

[14]Szabo, B. A., and Babuska, I., *Finite Element Analysis,* 1st ed., Wiley, New York, 1991, pp. 95-117.

[15]Kasagi, A., and Sridharan, S., "Postbuckling Analysis of Layered Composites Using p-Version Finite Strips," *International Journal of Numerical Methods in Engineering,* Vol. 33, No. 10, 1992, pp. 2091-2107.